PERGAMON

International Journal of Heat and Mass Transfer 45 (2002) 1951–1964

International Journal of HEAT and MASS TRANSFER

www.elsevier.com/locate/ijhmt

Multiple transient point heat sources identification in heat diffusion: application to experimental 2D problems

Frédéric Lefèvre, Christophe Le Niliot *

Institut Universitarie des Systemes IUSTI, UMR CNRS 6595, Technopôle de Château Gombert, 5, Rue Enrico Fermi, 13 453 Marseille Cedex 13, France

Received 24 March 2001

Abstract

This paper deals with an inverse problem, which consists of the experimental identification of line heat sources in a homogeneous solid in transient heat conduction. The location and strength of the line heat sources are both unknown. For a single source we examine the case of a source which moves in the system during the experiment. The identification procedure is based on a boundary integral formulation using transient fundamental solutions. The discretized problem is non-linear if the location of the line heat sources is unknown. In order to solve the problem we use an iterative procedure to minimize a cost function comparing the modelled heat source term and the measurements. The proposed numerical approach is applied to experimental 2D examples using measurements provided by an infrared scanner for surface temperatures and heat fluxes. In some particular examples, internal thermocouples can be used. A time regularization procedure associated to future time-steps is used to correctly solve the ill-posed problem.

1. Introduction

In the last few years, the inverse heat conduction problem (IHCP) has been the subject of a lot of works in various fields of research. Domains such as unknown boundary conditions reconstruction or parameters identification have been widely investigated. Paradoxically, the bibliography on the heat source term identification in the fundamentals equation of the heat transfers is quite small. This problem has nevertheless some interesting applications in various branches of engineering and science. For example, the knowledge of the heat generated by buried nuclear or chemical waste is essential to prevent environmental disaster. In this case, since the internal measurements are difficult or even dangerous, it is interesting to develop a method using only surface measurements to reconstruct the heat source term. Other applications of such a method can be interesting in the domain of non-destructive control, for example the control of pre-stressed concrete bridge structure damaged by steel corrosion. The steel rods, heated by Joule effect can be assimilated to point heat sources in a 2D section. By filming the bridge with an infrared scanner, we obtain the superficial temperature and heat flux field on the bridge boundaries. The aim is to identify the heat dissipated by Joule effect in the steel rods and their location using superficial measurements only in order to estimate their corrosion level.

In the present work, we propose the boundary element method (BEM) for the heat source term identification considered here as a discontinuous set of point heat sources at unknown location and unknown strength. Different authors working on point heat source identification propose methods such as adjoint method [1] or finite element method (FEM) [2]. In these two cases, the location of the point heat sources must be known to solve the inverse problem of strength identification. Recently Abou Khachfe [3] proposes the FEM associated to conjugate gradient algorithm to cope with the location and strength identification of multiple point heat sources. This method has been tested on a 2D experiment and gives good results for the identification of

* Corresponding author. Tel.: +33-04-9110-6886; fax: +33-04-9110-6969.

E-mail addresses: lefevre@iusti.univ-mrs.fr (F. Lefèvre), leniliot@iusti.univ-mrs.fr (C. Le Niliot).

0017-9310/02/$ - see front matter
PII: S0017-9310(01)00299-X

Nomenclature

$\mathbf{A}$	linear system matrix
B	second member vector
d	distance from the line heat source (mm)
g	heat source
g	algebraic line heat source strength
$\mathscr{G}, \mathscr{H}$	matrices for transient BEM
h	heat transfer coefficient
$\mathscr{I}$	matrix for point source treatment
K	number of point sources
L	square bar length
N	boundary element number
N'	internal points number
P	heat flux vector
$\mathbf{Q}$	time regularization matrix
T	temperature vector
R	number of future time-steps
S	source strengths vector
t	time
U	vector of the unknowns
W	transient BEM vector
x, y	Cartesian co-ordinates
X	co-ordinates vector

Greek symbols

Δ	algebraic error
Γ	boundary of the diffusive domain
Ω	diffusive domain
α	thermal diffusivity
λ	thermal conductivity
ε	emissivity
φ	measured heat flux (W m^2)
θ	temperature in Celsius (°C)
σ	standard deviation
Θ	vector for the location identification
η	time regularization coefficient

Subscripts

∞	ambient conditions

Superscripts

$\hat{}$	least squares solution
$\sim$	approximated heat source contribution
$'$	internal points

Abbreviations

BEM	boundary element method
FEM	finite element method
c.c.	curvilinear co-ordinates
t_c	thermocouple
Nu	Nusselt number
Pr	Prandtl number
Gr	Grashoff number

two static sources. In [4], we have proposed the BEM to identify both the location and the strength of point heat sources in the steady case. This method tested on a 2D experiment gives good results for the simultaneous estimation of four sources.

In a previous work we have presented the results of a transient experiment for point heat source estimation in 2D. This method proposed in [5] is available only in the case of a single source. The location estimation procedure, based on an iterative partitioning of the domain; it does not use directly the BEM for location estimation but the estimated strength of two artificial sources placed in two parts of the domain. The part of the domain which contains the source with the lower strength is eliminated at the next iteration. At the end of the process we have an estimation of the source location. This approach is available only in the case of a single static source but can be used with any method which permits a strength estimation of two sources when their location is known.

In a recent work [6], we have proposed a numerical method to identify the location and the strength of multiple static heat sources in transient heat conduction. This method can cope also with the identification of a moving source in 2D or 3D domains. Compared to the location estimation procedure proposed in [5], the approach uses the BEM to build the cost function for the location estimation procedure. This approach comparing the modelled heat source term and the measurements allows various configurations such as multiple static sources or moving sources.

BEM is well adapted to point heat source treatment because it does not require any refined mesh around the point heat source as in FEM. Indeed, for BEM taking into account different locations for a point heat source leads to a log function calculation of the co-ordinates in steady case and incomplete gamma function calculation of the co-ordinates in transient case.

In the present work we propose to test our approach on 2D experiments for the case of multiple static heat sources and for the case of a moving heat source. 3D applications are difficult to perform due to experimental problems to produce a point source with a significant strength. In our 2D applications the boundary measurements are given by an infrared scanner, which permits in most cases to avoid internal measurements. Compared to the experiment presented in [5], which concerned a single source, we propose here the estima-

tion of five heat sources activated at the same time using boundary measurements only. An experimental result for location estimation of a moving heat source is also presented.

This paper is divided in three parts. The first one describes in detail the experimental process. Two different experiments have been set up, one for the multiple static heat sources case and the other for the case of a single moving heat source. The second part describes briefly the method used to identify the location and the strength of the point heat sources. All the details concerning this method can be found in [6]. The third part is devoted to the experimental results.

2. 2D experiments using infrared thermographic data and internal temperatures

In order to test the identification method proposed in [6], two experiments have been set up. The experimental designs are two long square bars, one for the multiple static heat sources case and the other for the case of a single moving heat source. The proposed experimental setup is very similar to the one proposed in [4]. The chosen material is cement which leads to a good resistance to fracture at the temperature reached in our experiment.

In the presented examples, different kinds of measurements can be used, it can be an extra boundary condition or the temperature given by some thermocouples. When it is possible the boundaries are scanned using an infrared scanner and the surface temperature field is measured. The surface heat flux associated to the measurements is used as an extra boundary condition. The heat flux is obtained associating the measured temperature field to a calculated non-linear heat transfer coefficient. Such restrictive boundary conditions are not essential to solve the inverse problem and some other boundary conditions can be applied on the boundaries. We present an example with a part of the boundary imperfectly insulated.

2.1. The experimental design

The experimental designs under investigation are two long square section bars of cement crossed in their longest dimension by KANTHAL® heating wires of 0.3 mm diameter. In the central section of a bar, the diffusion system is assumed bi-dimensional. Considering the heating wires diameter (0.3 mm) compared to the section of a bar (50×50 mm^2), the heat generation can be approximated by a point in a section. The KANTHAL® wires are heated by Joule effect. The current is imposed by some independent power supplies, which are driven by a computer in order to control the strength variations. If we call L the length of the heating wire, the imposed strength of the source is: $g(t) = \text{current}(t) \times \text{voltage}(t)/L$.

The bar is fixed vertically on an optical bench (cf. Fig. 1). The surface temperature is measured using the

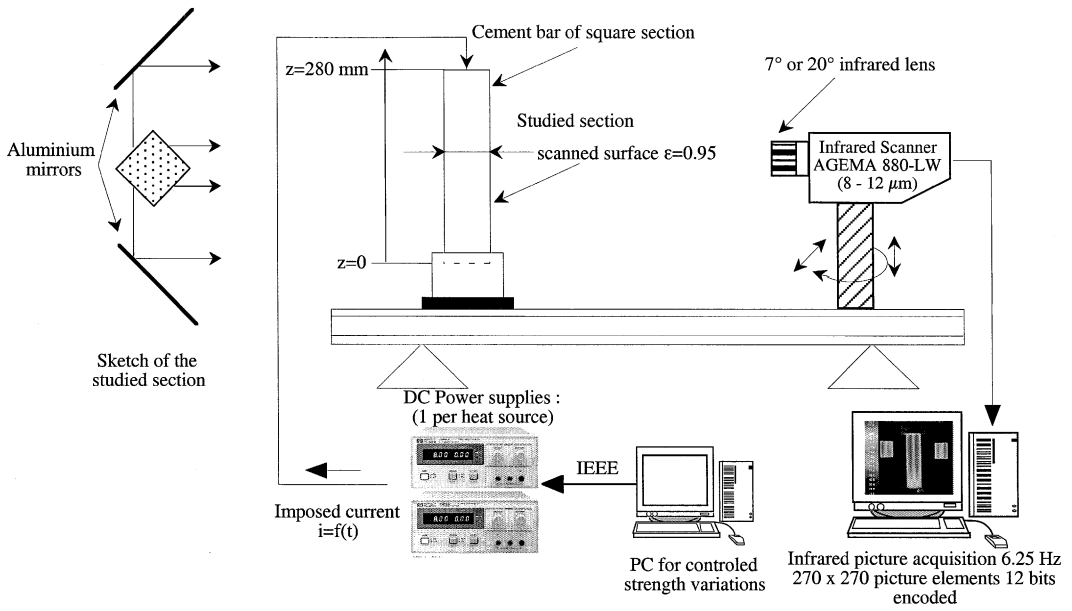

Fig. 1. The experimental setup scheme.

infrared scanner, an AGEMA® 880 LW, which is placed on the same bench. The infrared pictures constituted of 270×270 pixels (picture elements) are hard disc recorded. The infrared scanner is calibrated at the laboratory using the procedures described in [7]. In the obtained infrared picture used as a data-file it is necessary to extract 40 values, which represents 10 boundary elements on each side of the bar. To obtain this information from the picture we use a quadratic interpolation over the concerned pixels and the average temperature is then calculated at the middle of the element. Compared to the steady experiments presented in [4], we have to use two aluminium mirrors in order to have the four sides on the same picture. In the steady case, we could scan the four faces one by one using a 7° lens, here we use a 20° lens. As a result the number of pixels for each face is quite low (40 compared to 200 in the steady case). All the surfaces are painted in black. The black paint emissivity ε is 0.95 in the wavelength range of the scanner: 8–12 μm.

Two different bars are used to test both the multiple static heat sources case and the moving heat source case. Their sections are displayed in Figs. 2 and 3. In the first domain, we can activate five different heating wires, four of them are located in the corners, the fifth one is located in the middle of the section. In the second section we find 16 heating wires located on a circle of centre g_0 and diameter 30 mm. The distance between two heating wires is constant and equal to 5.85 mm. The heating wires are activated successively in order to simulate a moving heat source.

In the section under investigation two sensors (t_{c_1} and t_{c_2}) can be found at 10 mm from a heating wire g_0 placed in the middle of the section (cf. Figs. 2 and 3). They are used to identify the thermal properties of the material using a method similar to the two linear probe

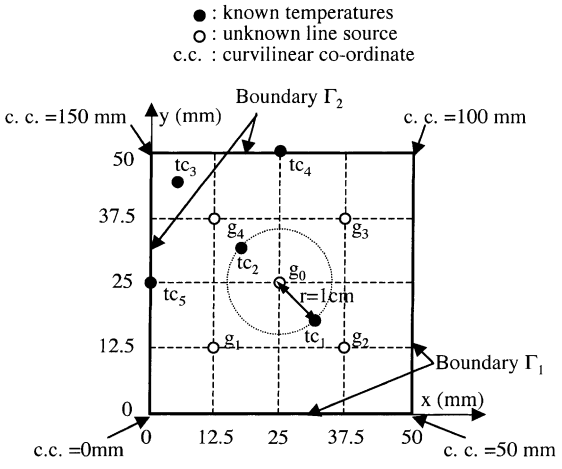

Fig. 2. The experimental section for the multiple static heat sources case.

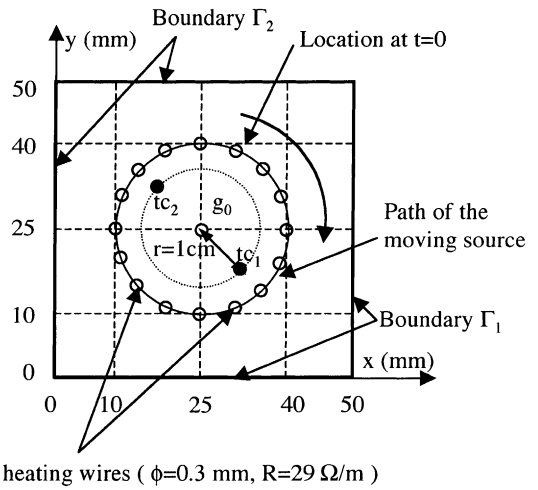

Fig. 3. The experimental section for the moving heat source.

method proposed in [8]. The thermal conductivity of the cement used for these experiments is $\lambda = 0.96$ W m^{-1} K^{-1}. The thermal diffusivity is equal to $\alpha = 5.3 \times 10^{-7}$ m^2 s^{-1}.

2.2. The experimental inverse problem

In this paragraph we present the boundary conditions associated to the measurements used to solve the inverse problem. The 2D section under investigation is discretized in 40 BEM linear elements. The inverse problem consists in identifying each activated heat source location and the associated strength. To cope with this problem we use different boundary conditions, either Γ_1 and Γ_2 are scanned or Γ_1 is scanned and Γ_2 is imperfectly insulated.

2.2.1. All the sides are scanned

In this case the temperature and the heat flux is known for each boundary element. The heat flux densities over the scanned surfaces are obtained as the sum of radiant and convective losses. For the radiant heat flux we have $\varphi_r = \varepsilon\sigma(\theta_r^4 - \theta_i^4)$ with θ_r the radiant ambient temperature in Kelvin and θ_i the measured temperature at element Γ_i of the scanned boundary. For the convective heat transfer coefficient h_c, we use the relation proposed by Elenbaas [9] for a short vertical cylinder in calm air. In the case of a cylinder of length L and diameter D we have:

$$Nu_D \exp\left(\frac{-2}{Nu_D}\right) = 0.6\left(Gr.Pr.\frac{D}{L}\right)_D^{1/4} \quad (1)$$

This correlation is used considering an average temperature along the studied section and for the diameter D equal to 50 mm. In Fig. 4, we present the heat transfer

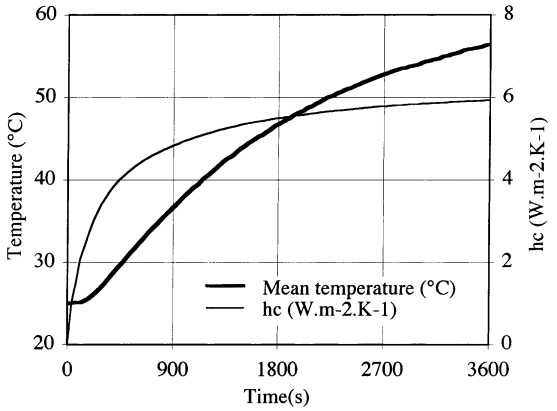

Fig. 4. Convection heat transfer coefficient h_c and mean temperature history on the scanned surface versus time for $g_0 = 100$ W m^{-1}, $\theta_\infty = 25$ °C.

coefficient evolution and the mean temperature evolution on the scanned surface versus time obtained for a constant strength of 100 W m^{-1} on g_0 and an air temperature of 25 °C.

The calculated heat transfer coefficient h_c is applied on each element and a local relation is used for the radiant heat flux. Including radiant and convective losses, the measured heat flux φ_i at boundary element Γ_i associated to the measured temperature θ_i is given by the relation:

$$\varphi_i(\theta_i) = \varepsilon\sigma\left(T_r^4 - T_i^4\right) + h_c(t)(\theta_\infty - \theta_i) \quad (2)$$

2.2.2. Two sides insulated

Compared to the inverse problem above described, the set of boundary conditions is different. Two sides are scanned and the two others are insulated with polystyrene slabs of 4 cm thickness. The thermal properties of the polystyrene (*roofmat solid foam*) are $\lambda = 0.029$ W m^{-1} K^{-1} and $\alpha = 4 \times 10^{-7}$ m^2 s^{-1}. The scheme of the heat transfer through the insulation is displayed in Fig. 5. A local time dependant heat losses coefficient $h_0(t)$ is calculated along the insulated boundary Γ_2 using a direct 2D simulation. $h_0(t)$ is the local ratio of the interface normal flux by the temperature difference between interface and outside environment. A 1D approach can be used for this type of problem but it is an inefficient model of the heat losses through the insulation because it does not take into account the 2D effects at the corner (c.c. = 0.15 m) and at the end of the insulation (c.c. = 0.2 m and c.c. = 0.1 m). As a result h_0 is not a global coefficient but a function of the curvilinear co-ordinate.

3. The point heat source identification procedure

In this part, we present briefly the iterative procedure for point heat sources identification in a domain for transient heat conduction, which means that both location and strength can be identified. This procedure is based on a BEM formulation, which permits to cope in a convenient way with point heat sources. BEM permits the strength identification (see [10]) using a sequential approach and can also cope with location identification (see [6]). The location identification procedure connects a linear strength identification procedure with a non-linear location identification procedure in an iterative process. The non-linear identification of the location can be global, using all the time-steps in the case of static sources or sequential using some future time-steps and a function specification method for moving sources.

3.1. The heat source strength identification

In this section we present our approach for the strength identification of point heat sources whose locations are known. The presented method uses sequential BEM and the future time-steps procedure. To solve the ill-posed problem we use the time regularization

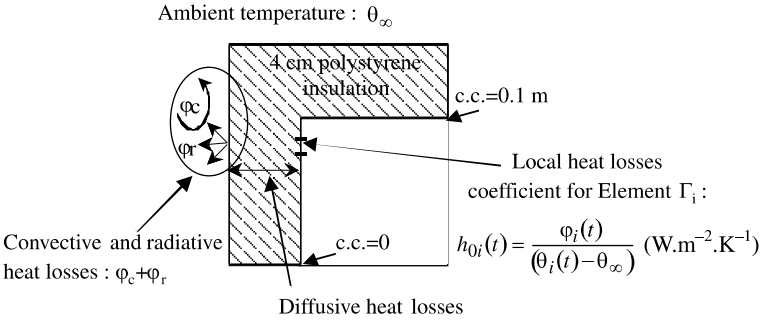

Fig. 5. Scheme of the heat transfer through the insulation.

procedure [12] over the future time-steps. All the details concerning the method can be found in [10].

If we consider a domain Ω of boundary Γ and if we discretize Γ in N elements constant over space and linear over time [11] at resolution time t_f the boundary integral equations can be assembled in a linear system. If we use R future time-steps at resolution time t_f we obtain the following system of simultaneous equations:

$$\mathscr{H}_{f,f+r}\begin{bmatrix} T_f \\ \vdots \\ T_{f+r} \end{bmatrix} = \mathscr{G}_{f,f+r}\begin{bmatrix} P_f \\ \vdots \\ P_{f+r} \end{bmatrix} + \mathscr{I}_{f,f+r}\begin{bmatrix} S_f \\ \vdots \\ S_{f+r} \end{bmatrix} - \begin{bmatrix} \begin{bmatrix} 0 \\ T'_f \end{bmatrix} \\ \vdots \\ \begin{bmatrix} 0 \\ T'_{f+r} \end{bmatrix} \end{bmatrix} + W_{f,f+r}. \tag{3}$$

Here, macro matrices $\mathscr{H}$ and $\mathscr{G}$ are $((N+N')\times(R+1), N\times(R+1))$ dimensioned and depends on the domain geometry, on the diffusivity α and on the time t_{f+r} $(0\leqslant r\leqslant R)$. Vector W is $(N+N')\times(R+1)$ dimensioned and contains all the information relative to the previous time-steps ($t<t_f$). T_{f+r} (P_{f+r}) is the N dimensioned vector of the temperatures (heat flux) at the boundary at time t_{f+r} $(0\leqslant r\leqslant R)$. Vectors T'_{f+r} are the vectors of the measured temperatures at the internal points. S_{f+r} is the vector of the K heat source strengths at time t_{f+r} $(0\leqslant r\leqslant R)$. Macro matrix $\mathscr{I}$ is $((N+N')\times(R+1), K\times(R+1))$ dimensioned and depends on the location of the heat sources. The locations are included in matrix $\mathscr{I}$ in a non-linear way through some incomplete gamma functions of the distance from the source to the considered boundary nodes.

If we assume that the point heat source locations are known as initially guessed (or updated) locations [10], system (3) is linear considering heat source strength identification. As a result matrix $\mathscr{I}_{f,f+r}$ can be computed and linear system (3) can be solved in the sense of vectors S_{f+r} $(0\leqslant r\leqslant R)$ identification. If we can find some boundary variables (at least one per element), which can be a prescribed temperature, a prescribed heat flux or both boundary variables prescribed, the number of unknown boundary variables can be reduced to $M\times(R+1)$. Under all these assumptions it is possible to arrange system (3) into the linear system:

$$\mathbf{A}U = B, \tag{4}$$

where $\mathbf{A}$ is a matrix of dimension $((N+N')\times(R+1), (M+K)\times(R+1))$, U is a vector of dimension $(M+K)\times(R+1)$ and B is a vector of dimension $(N+N')\times(R+1)$. In the general case we have more measurements than unknowns and U has to minimize a cost function $J(U)$.

If we use a time regularization procedure, the classical cost function is modified and U has to minimize function $J(U)$ given below:

$$J(U) = \|\mathbf{A}U - B\| + \eta\|\mathbf{Q}U\|. \tag{5}$$

Here $\mathbf{Q}$ is the time regularization matrix of dimension $((M+K)\times(R+1), (M+K)\times(R+1))$ and η is a coefficient adjusting the amplitude of $\mathbf{Q}$.

The regularization procedure, used to reduce excursions into the unknown function, is based on the regularization operator recommended by Tikhonov [12]. In all the following we will use a second-order regularization which preserve the average of the identified function. If we apply the least squares method to minimize function (5), this leads to vector $\hat{U}$ solution of the square linear system:

$$(\mathbf{A}^{\mathrm{T}}\mathbf{A} + \eta\mathbf{Q}^{\mathrm{T}}\mathbf{Q})\hat{U} = \mathbf{A}^{\mathrm{T}}\mathbf{B}. \tag{6}$$

A resolution of (6) is performed at each resolution time t_f. In a strength identification procedure we extract from vector $\hat{U}$ components the components $\hat{U}_f$ of the unknowns at time t_f; the other components $(\hat{U}_{f+1},\ldots,\hat{U}_{f+r})$ of $\hat{U}$ being ignored. If the locations are wrong, the error in fit to measured data is important. This error is our criterion to find the correct locations of the heat sources.

3.2. The heat source location identification procedure

Contrary to the strength identification problem, the location identification problem is non-linear because macro matrix $\mathscr{I}$ contains non-linear functions of the sources co-ordinates. Nevertheless, it is possible to calculate analytically the first derivatives of these functions with respect to the co-ordinates. We can then apply a Newton method to find the location of the sources. As the co-ordinates can be constant or time dependent according as the sources are static or not, we have developed two different location identification procedures. The first one concerns the multiple static heat sources case and the second one the single moving heat source case.

3.2.1. The case of multiple static sources

In this section we consider the case where the heat sources are supposed to be static during the experiment. Considering system (3) let us introduce two vectors, $\hat{\boldsymbol{\Theta}}_{1,F}$ and $\tilde{\boldsymbol{\Theta}}_{1,F}$, respectively, the vector of the boundary variables contribution and the vector of the heat sources contribution for all the F time-steps, from time t_1 to time t_F. These vectors are the results of the following matrices operations:

$$\hat{\boldsymbol{\Theta}}_{1,F} = \mathscr{H}_{1,F}\begin{bmatrix}\hat{T}_1\\ \vdots\\ \hat{T}_F\end{bmatrix} - \mathscr{G}_{1,F}\begin{bmatrix}\hat{P}_1\\ \vdots\\ \hat{P}_F\end{bmatrix} + \begin{bmatrix}\begin{bmatrix}0\\ T'_1\end{bmatrix}\\ \vdots\\ \begin{bmatrix}0\\ T'_{\mathrm{F}}\end{bmatrix}\end{bmatrix} \quad \text{and}$$

$$\tilde{\boldsymbol{\Theta}}_{1,F} = \mathscr{I}_{1,F}\begin{bmatrix}\hat{S}_1\\ \vdots\\ \hat{S}_F\end{bmatrix}. \tag{7}$$

As the co-ordinates are assumed constants over all the time-steps, this procedure is not sequential but global and vectors $\hat{\boldsymbol{\Theta}}_{1,F}$ and $\tilde{\boldsymbol{\Theta}}_{1,F}$ are $(N+N')\times F$ dimensioned. For location identification, the aim is to find an estimation of vector X, which contains the sources co-ordinates. An estimation of vector X is found solving the following optimization problem:

$$\hat{X} = \arg\{\min \|\hat{\boldsymbol{\Theta}}_{1,F} - \tilde{\boldsymbol{\Theta}}_{1,F}\|\}, \tag{8}$$

where X is a vector of dimension $2\times K$ in 2D ($3\times K$ in 3D) containing the estimated co-ordinates of the K heat sources. The identification method consists in a first-order approximation of the difference $(\hat{\boldsymbol{\Theta}}_{1,F} - \tilde{\boldsymbol{\Theta}}_{1,F})$ with respect to the co-ordinates in order to evaluate the errors ΔX on the initially guessed co-ordinates or updated co-ordinates. An estimation of the error is found solving:

$$(\hat{\boldsymbol{\Theta}}_{1,F} - \tilde{\boldsymbol{\Theta}}_{1,F}) = \mathscr{D}_{1,F}\Delta X. \tag{9}$$

Here $\mathscr{D}_{1,F}$ is the matrix of the first derivatives of $(\hat{\boldsymbol{\Theta}}_{1,F} - \tilde{\boldsymbol{\Theta}}_{1,F})$ with respect to the co-ordinates of the sources. The latter system of equations is solved in the sense of the least squares and the co-ordinates are updated such as: $\hat{X}_{\text{updated}} = \hat{X}_{\text{initial}} + \Delta\hat{X}$. The updated co-ordinates are used to solve the strength identification problem. At the end of the iterative process, $\|\hat{\boldsymbol{\Theta}}_{1,F} - \tilde{\boldsymbol{\Theta}}_{1,F}\|$ is minimum with the identified locations and strengths. As the inverse problem is unstable considering the errors on the co-ordinates Δx and Δy, the latter are controlled in order to avoid an intermediate location out of the domain. The direction given by the successive location procedure is preserved but the maximum distance covered between two successive locations is imposed at 1/5 of Ω characteristic dimension. This procedure reduces the excursions of the sources out of the domain; thus the number of iterations is reduced. Nevertheless if during the iterative process a location is found out of the domain, a new location is randomly imposed in the domain.

3.2.2. The case of a single moving heat source

In this case, as the co-ordinates are function of time, the method is sequential. Compared to the above-mentioned procedure, the iterative process occurs at each time-step to identify both the strength and the location of the source. At resolution time t_f the expression of $\hat{\boldsymbol{\Theta}}$ and $\tilde{\boldsymbol{\Theta}}$, over R future time steps is:

$$\hat{\boldsymbol{\Theta}}_{f,f+r} = \mathscr{H}_{f,f+r}\begin{bmatrix}\hat{T}_f\\ \vdots\\ \hat{T}_{f+r}\end{bmatrix} - \mathscr{G}_{f,f+r}\begin{bmatrix}\hat{P}_f\\ \vdots\\ \hat{P}_{f+r}\end{bmatrix} - W_{f,f+r} \quad \text{and}$$

$$\tilde{\boldsymbol{\Theta}}_{f,f+r} = \mathscr{I}_{f,f+r}\begin{bmatrix}\hat{S}_f\\ \vdots\\ \hat{S}_{f+r}\end{bmatrix}. \tag{10}$$

Here $W_{f,f+r}$ is a vector containing all the information from the previous time-steps and also the temperatures measured at the N' internal points. The procedure is here sequential and vectors $\hat{\boldsymbol{\Theta}}_{f,f+r}$ and $\tilde{\boldsymbol{\Theta}}_{f,f+r}$ are $(N+N')\times(R+1)$ dimensioned. The aim is to find a vector X_f containing the source co-ordinates at time t_f. An estimation $\hat{X}_f$ of vector X_f can be found by solving the optimization problem:

$$\hat{X}_f = \arg\{\min \|\hat{\boldsymbol{\Theta}}_{f,f+r} - \tilde{\boldsymbol{\Theta}}_{f,f+r}\|\}. \tag{11}$$

The location identification method consists in a first-order approximation of the difference $(\hat{\boldsymbol{\Theta}}_{f,f+r} - \tilde{\boldsymbol{\Theta}}_{f,f+r})$ with respect to the co-ordinates in order to evaluate the errors on the initially guessed co-ordinates at each future time-step. The co-ordinates are updated and used to solve the linear strength identification problem defined in Section 3.1 at time-step f. In order to reduce the sensitivity to measurements errors, we use the function specification method recommended by Beck et al. [13] in the strength identification procedure. We assume that the co-ordinates are constants over the R future time-steps to identify the strength of the moving heat source for the strength identification procedure. At the end of the iterative process, $\|\hat{\boldsymbol{\Theta}}_{f,f+r} - \tilde{\boldsymbol{\Theta}}_{f,f+r}\|$ is minimum with the identified location and strength at time-step t_f and the process can be resumed for time t_{f+1}.

4. The experimental results

In this paragraph we present some experimental results obtained using our method. The examples are chosen to illustrate our approach but they do not constitute an exhaustive test of the identification procedure. Two different cases are examined relative to the identification of multiple static heat sources and to a moving heat source.

Table 1
Identified co-ordinates for a four sources case involving sources g_1–g_4

Source	Identified x, y		Co-ordinates errors		d (mm)
	x (mm)	y (mm)	Δx (mm)	Δy (mm)	
g_1	12.6	12.3	0.1	−0.2	0.26
g_2	36.7	13.3	−0.8	0.8	1.14
g_3	37.0	37.1	−0.5	−0.4	0.70
g_4	13.1	36.6	0.6	−0.9	1.06

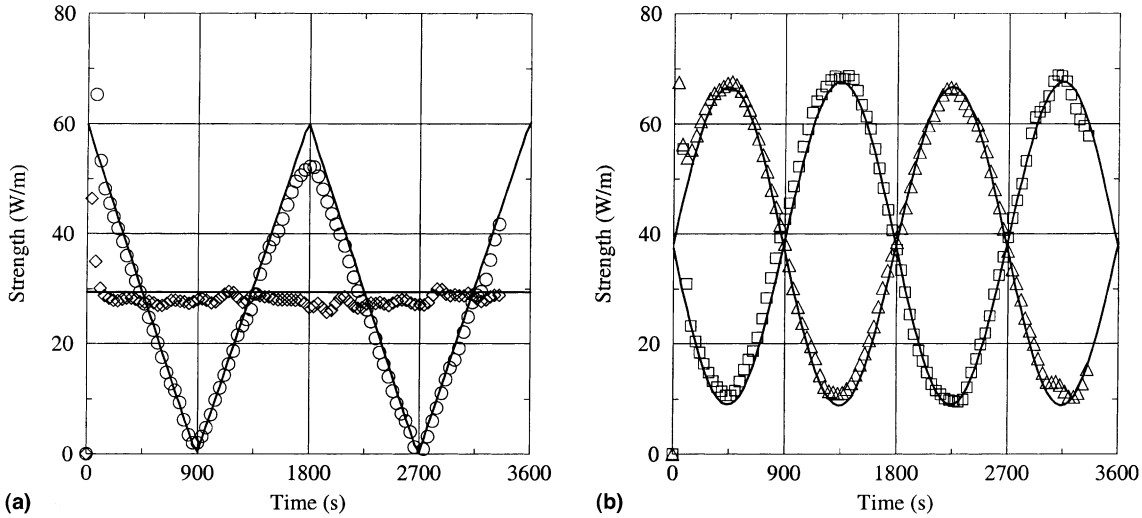

Fig. 6. Identified strengths (W m^{-1}) versus time (s) using the locations given in Table 1, $R = 6$: (a) g_1 (◇) and g_3 (◯), (b) g_2 (□) and g_4 (△), (—— real strengths).

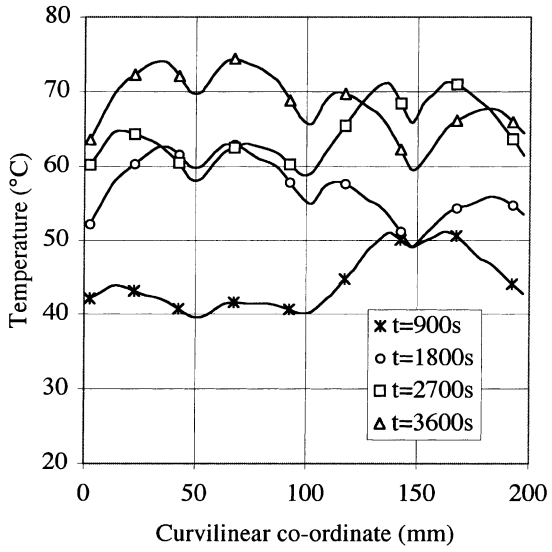

Fig. 7. Temperature evolution versus curvilinear co-ordinate at different time-steps.

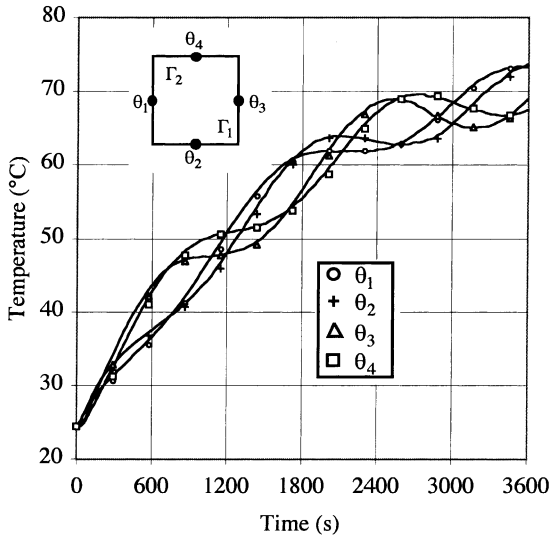

Fig. 8. Temperature evolution versus time in the middle of each face.

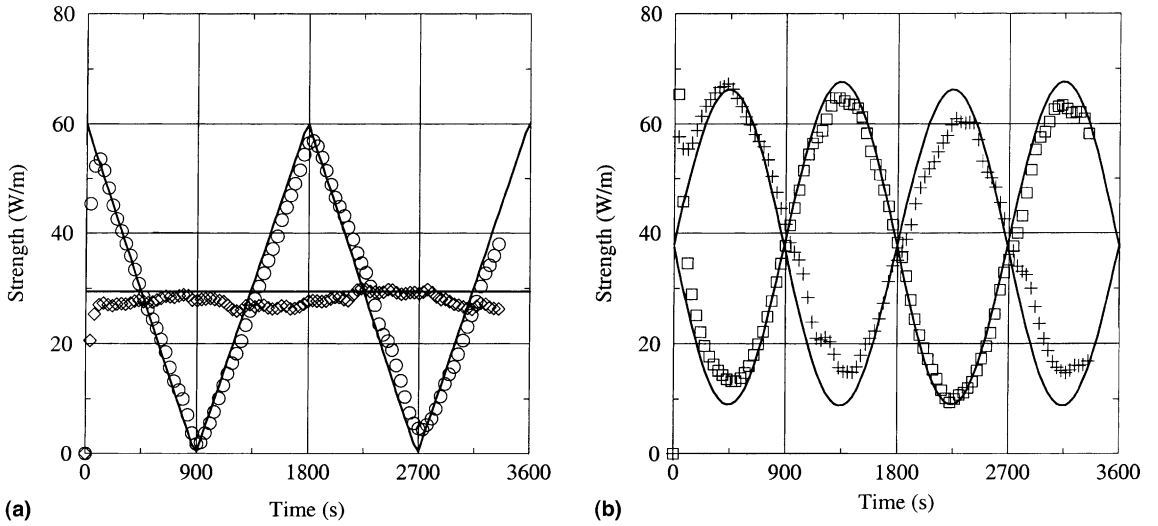

Fig. 9. Identified strengths (W m^{-1}) versus time (s) using the locations given in Table 2, $R = 6$: (a) g_1 (◇) and g_3 (◯); (b) g_2 (□) and g_0 (+), (—— real strengths).

4.1. The multiple static heat sources case

This part is relative to the domain described in Fig. 2. We present some results concerning two different sets of boundary conditions. In the first case, the four faces of the bar are scanned, which gives both temperature and heat flux on Γ_1 and Γ_2. In the second case, only Γ_1 is scanned and Γ_2 is imperfectly insulated. In this last example as we have less information in the insulated corner some thermocouples are used as internal temperatures.The experiments last 3600 s and the time-step used for the identification is $\Delta t = 36$ s. Six future time-steps are used for the strength identification.

4.1.1. All the sides are scanned

The first example concerns the identification of four sources (g_1–g_4) located in the four corners of the square bar. The sources are activated with different strength variations: $g_2(t)$ and $g_4(t)$ are sinusoidal and their phases are opposed, $g_1(t)$ is constant and $g_3(t)$ is triangular. The identified co-ordinates are displayed in Table 1. Distance d, given in mm, is the distance between the identified and the experimental source ($d = \sqrt{\Delta x^2 + \Delta y^2}$). As we can see in Table 1, the location identification is accurate with a maximum distance between the identified and experimental source of 1.1 mm.

The results concerning the strength identification are displayed in Fig. 6. They are very satisfactory with an error lower than 5% on the identified strength.

In the above-mentioned identification, only boundary measurements are used. The temperature field is presented versus curvilinear co-ordinates at four different time-steps in Fig. 7. In Fig. 8 we present the evolution of the temperature versus time at the boundary for four points located in the middle of each face. These measurements are obtained using 100 infrared pictures.

The second example concerns an other identification of four sources, but the configuration is different. Compared to the previous case source g_4 is replaced by source g_0 located in the centre of the domain. The strength variations of g_1–g_3 are the same as in the first example and g_0 has the same strength variation as g_4 (see Fig. 9).

This case is more difficult than the previous one because the four sources are closer to each other. Let us consider the singular value decomposition of the

Table 2
Identified co-ordinates for a four sources case involving sources g_0–g_3

Source	Identified x, y		Co-ordinates errors		d (mm)
	x (mm)	y (mm)	Δx (mm)	Δy (mm)	
g_1	14.0	11.9	1.5	−0.6	1.62
g_2	36.3	13.2	−1.2	0.7	1.41
g_3	36.5	36.4	−1.0	−1.1	1.46
g_0	23.1	26.2	−1.9	1.2	2.23

Table 3
Identified co-ordinates for a five sources case involving sources g_0–g_4

Source	Identified x, y		Co-ordinates errors		d (mm)
	x (mm)	y (mm)	Δx (mm)	Δy (mm)	
g_0	21.4	24.7	−3.6	−0.3	3.57
g_1	12.7	10.4	0.2	−2.1	2.12
g_2	36.0	13.0	−1.5	0.5	1.60
g_3	36.3	36.3	−1.2	−1.2	1.70
g_4	12.6	37.8	0.1	0.3	0.31

strength identification matrix **A** (see Eq. (4)) and the associated condition number [14], defined as the ratio of the largest singular value to the smallest one. For a well-conditioned matrix this number will be close to one. Conversely, a matrix is ill-conditioned if its condition number is too large. The first configuration (g_1–g_4) leads to a condition number of about 4×10^5 without regularization. In the second example (g_0–g_3), the value grows up to 1.5×10^{13}. It shows that the matrix is worse ill-conditioned in the second case, which means that the measurement errors will be amplified. In the corners of the square bar, the temperature measurements are less accurate, which is a consequence of an imperfect focus of the infrared scanner. This inaccurate information introduced in the second member leads to important errors in the strength identification.

Table 2 presents the location identification results. The results are less accurate as in the previous case. The error on the location of g_1–g_3 is about 1.5 mm. For g_0, the distance between the experimental source and the identified source grows up to 2.2 mm, which is due to the sensitivity coefficients to the co-ordinates, which are lower for g_0 than for the sources located in the corners of the square section.

In Fig. 9, we present the identified strengths with the locations given in Table 2. The results are satisfactory but less accurate than in the first case. The errors on the sources strengths compensate each other. For example, if we consider sources g_0 and g_1 at time $t = 1300$ s, we see that the strength of g_1 is lower than expected when the one of g_0 is higher than expected.

The third and last example involves five sources (g_0–g_4). The strength variations of g_1–g_4 are the same as in the first example and $\mathrm{g}_0(t)$ is constant. In this case the problem is more difficult with a condition number of 1.5×10^{14}. The results of the location identification are given in Table 3. As in the previous case the error on the identified location of g_0 is more important than for the other one. As the sources are very close, the errors on the locations identifications leads to errors on the strengths much more important than in the first examples for all the sources.

The identified strengths displayed in Fig. 10 show that the results are less satisfactory with a maximum

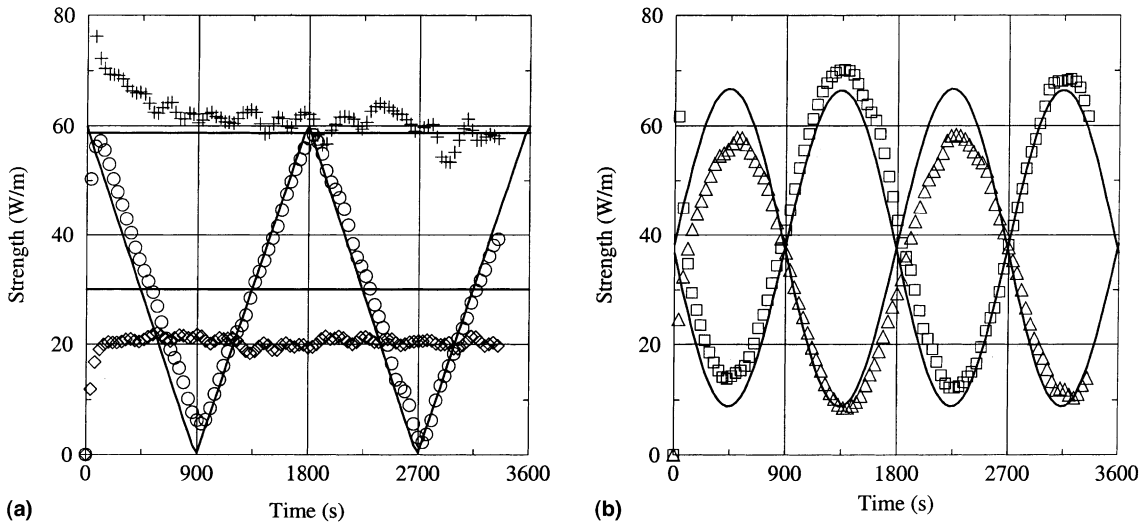

Fig. 10. Identified strengths (W m^{-1}) versus time (s) using the locations given in Table 3, $R = 6$: (a) g_1 (◇), g_3 (◯) and g_0 (+); (b) g_2 (□) and g_4 (△), (—— real strengths).

Table 4
Identified co-ordinates for a four sources case involving sources g_1–g_4, Γ_2 is insulated

Source	Identified x, y		Co-ordinates errors		d (mm)
	x (mm)	y (mm)	Δx (mm)	Δy (mm)	
g_1	13.4	13.1	0.9	0.6	1.06
g_2	37.2	12.6	−0.3	0.1	0.27
g_3	36.0	36.1	−1.5	−1.4	2.09
g_4	13.4	35.9	0.9	−1.6	1.82

error of 30% for the strength identification of g_1. As in the previous case, the errors on the sources strengths compensate each other for global energy conservation. These results are due to the error on the location identification and to the ill-posed character of the strength identification procedure.

4.1.2. Two sides insulated

In this part, we present a result obtained when we have less information on a part of the boundary. Here temperature and heat flux are given on Γ_1, when Γ_2 is insulated. The boundary condition on Γ_2 is known to be Fourier boundary condition but no extra information is given. As Γ_2 is imperfectly insulated we calculate the heat losses coefficient using a direct 2D computation. This coefficient could be estimated using a boundary condition estimation procedure, but in this case it means that we can control the heat source which is not our aim.

Three thermocouples, t_{c_3}–t_{c_5} (see Fig. 2), are used. They are located in the insulated part of the domain where there is a lack of information. The presented result involves the sources located in the corners of the square section (g_1–g_4). The sources are activated with different strength variations: $g_1(t)$ and $g_3(t)$ are sinusoidal and their phases are opposed, $g_2(t)$ is constant and $g_4(t)$ is triangular. The identified locations are displayed in Table 4, and the corresponding strengths are presented in Fig. 11. The results are very satisfactory for g_2, which is in the scanned corner with an error on the location identification of 0.3 mm. For the other sources the results are although good with a maximum error $d = 2.1$ mm on the source g_3 identification.

4.1.3. Influence of the initial location

Through an example we propose to examine the influence of the initial location on the results of the identification procedure. Let us examine the abovementioned case with sources g_1–g_4 activated. The previous identification has been performed using the initial locations at the centre of the bar, at four different locations located at 0.1 mm of the centre. The results after 5 iterations are given in Table 1. In order to test the stability of the results to initial locations the path covered by the identified locations during the iterative

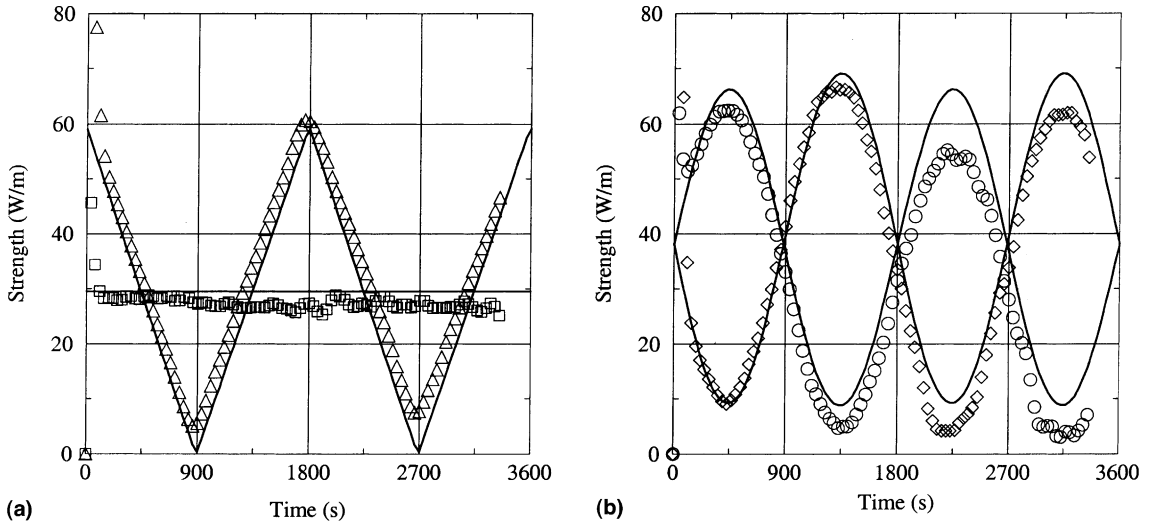

Fig. 11. Identified strengths (W m^{-1}) versus time (s) using the locations given in Table 4, $R = 6$: (a) g_2 (□) and g_4 (△); (b) g_1 (◇) and g_3 (○), (—— real strengths).

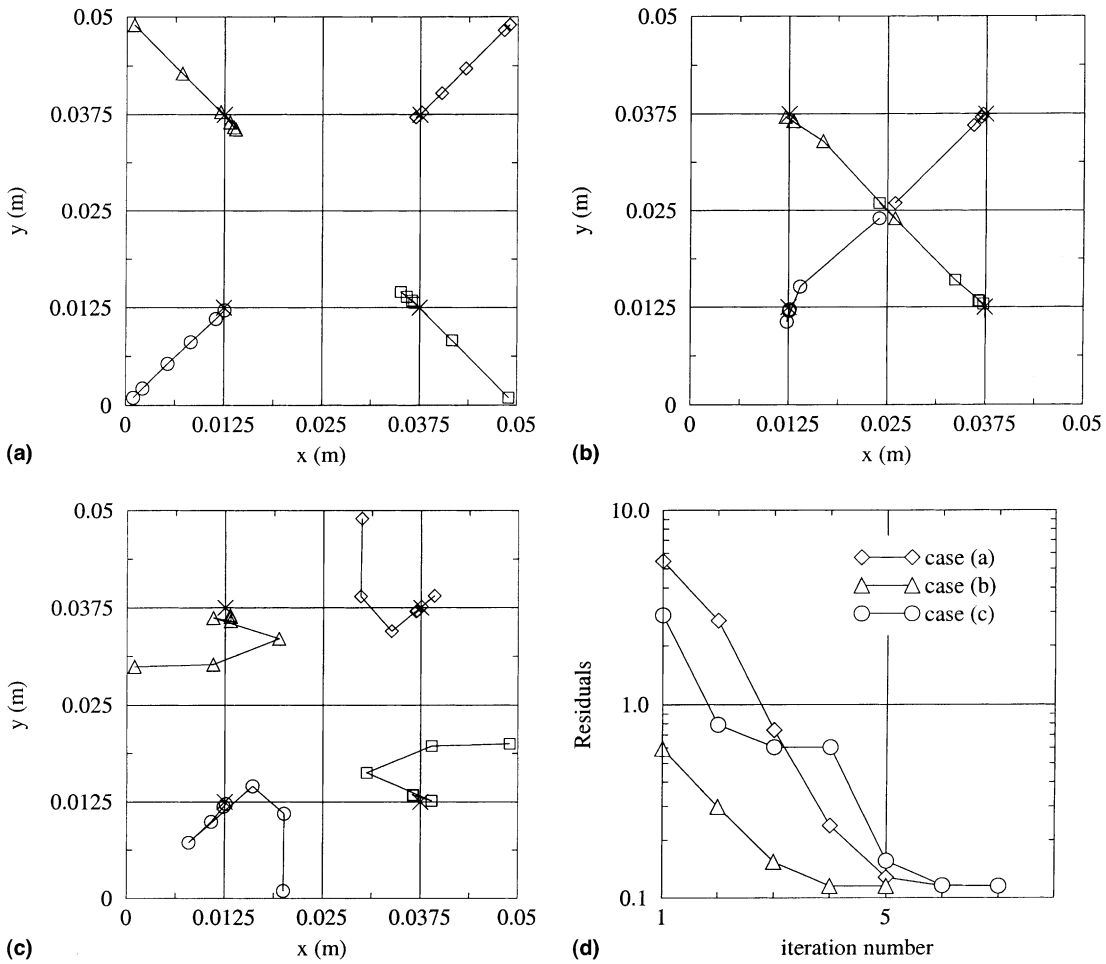

Fig. 12. Path followed by the searched heat sources (g_1 (◯), g_2 (□), g_3 (◇) and g_4 (△)) during the iterative process for different initial locations (∗ real location). (a) g_1 (1;1) g_2 (49;1) g_3 (49;49) g_4 (1;49), (b) g_1 (24.9;24.9) g_2 (24.9;25.1) g_3 (25.1;25.1) g_4 (25.1;24.9), (c) g_1 (20;1) g_2 (49;20) g_3 (30;49) g_4 (1;30), (d) Residuals versus the iteration number for cases (a)–(c).

process is recorded. The results are displayed in Fig. 12 for three different initial locations (in the corners, at the centre ...). The stopping criterion is here of 0.15 mm, which corresponds to a radius of the heating wires. All the obtained final locations are the same within 0.1 mm. The number of iteration is low and varies from 5 for case (a) to 7 for case (c). The value of the residual $\|\hat{\boldsymbol{\Theta}}_{1,F} - \tilde{\boldsymbol{\Theta}}_{1,F}\|$ is given in figure (d) versus the iteration number. This number declines with the number of iteration, which validates the iterative method in this particular case.

In our previous works, see [4] for steady state heat conduction using some experimental measurements and see [6] for transient heat conduction using simulated measurement, we have presented some results when the number of sources is unknown. As shown in [4] the case of a declared number of sources (K) inferior to the real number can by eliminated quite easily. In this case the residual is superior to the expected residual using the measurement errors which shows that we have an incorrect number K. For the example presented in Fig. 12, if the declared number of sources (K) is superior to the real number, the number of iterations increases dramatically but the process still converge with five and six sources whatever the initial location. The extra sources are then located in the corners of the domain with a low strength. This particular location is found in order to compensate the measurement errors due to an imperfect focus of the scanner at the corners. As a result the residual $\|\hat{\boldsymbol{\Theta}}_{1,F} - \tilde{\boldsymbol{\Theta}}_{1,F}\|$ decreases as the number of extra sources increases. When the number of unknowns is equal to the numbers of data the residual are null because all the extra sources (sinks) are acting as little generators offsetting exactly the measurements errors.

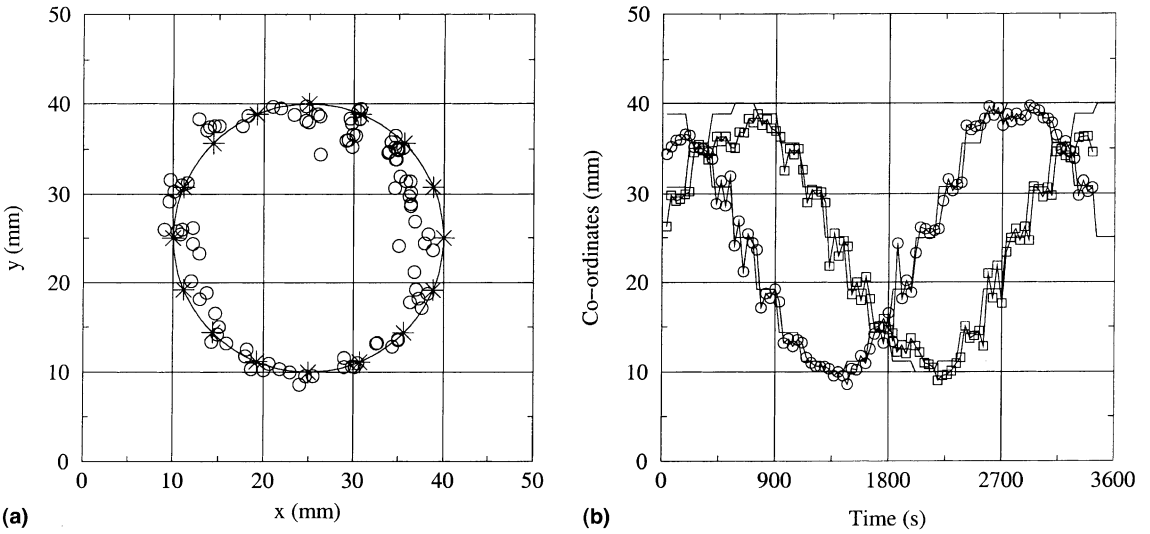

Fig. 13. (a) Identified locations (◯) of a moving source at each time step, $R = 4$, ($*$ real location). (b) Identified co-ordinates x (□) and y (◯), (—— real values).

4.2. The moving heat source case

This part is relative to the domain described in Fig. 3. The moving point heat source is simulated by 16 heating wires activated successively. In the presented examples, all the boundaries are scanned and no thermocouple used.The experiment lasted 3600 s and we use four future time-steps to identify both the path and the strength of the point heat source. In the first example, the moving heat source describes one circle in 48 min, which represents an average speed of 118 mm/h. Each heating wire is activated with a constant strength. The identified path is given in Fig. 13. As we can see, the identified locations at each time-step are slightly dispersed around the real locations. The average distance between the real location and the identified location is $d = 2.5$ mm. As we use a function specification method for the co-ordinates, the method fails to reconstruct the stepwise location variations.

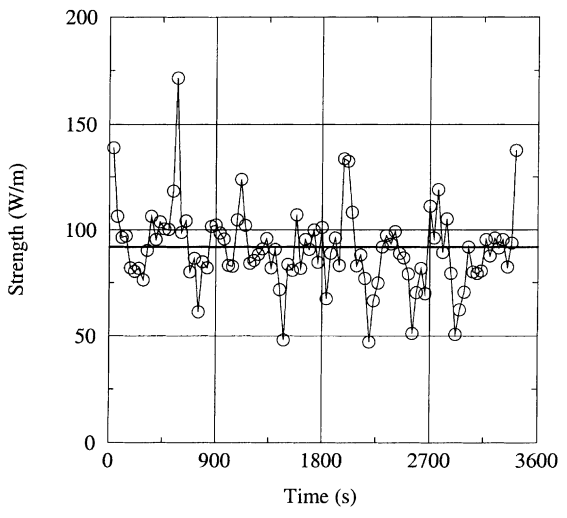

Fig. 14. Strength identification using the identified locations at each time-step, $R = 4$.

In Fig. 14, we present the identified strengths at each time step. Compared to the multiple heat sources identification case, the identified strength is not smooth. Let us introduce the standard deviation σ between the real strengths S_f and the identified strengths $\hat{S}_f$ $(1 \leqslant f \leqslant F)$.

The standard deviation σ is equal to 18.6 W m^{-1}, which is very important. This is due to the error on the location identification. Nevertheless, the average of the difference between the real strength and the identified strength on all the time steps is lower than 1.5 W m^{-1}, which shows that the global energy is well recovered.

In the second example, the moving heat source describes one circle in 28.8 min, which represents an average speed of 196 mm/h. The strength variation is the same as in the previous example. In this case, the identified locations are more dispersed around the real locations (see Fig. 15(a)), the average distance between the real locations and the identified locations is about $d = 3$ mm. As a result, the standard deviation between the real strength and the identified strength grew up and is equal to $\sigma = 24.2$ W m^{-1} (see Fig. 15(b)). In this last part only constant variations of the strength are presented but of course we can have any shape of variation because no a priori information is given on the strength history.

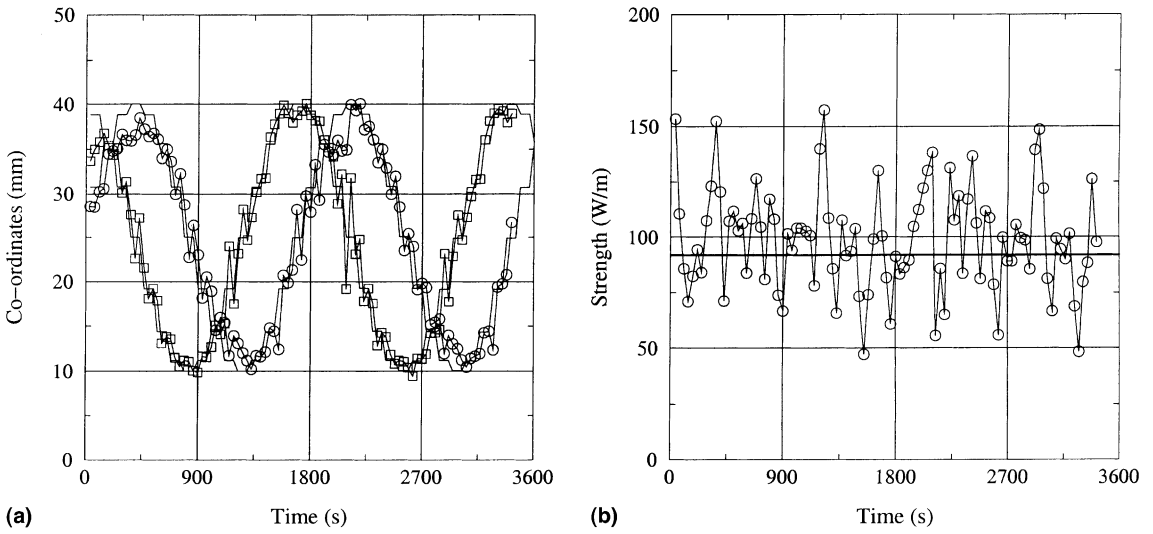

Fig. 15. (a) Identified co-ordinates x (□) and y (◯), (—— real values). (b) Identified strengths using the identified locations at each time step, $R = 4$.

5. Conclusion

In order to test our previous numerical works about heat source identifications, we set up a 2D experiment, which allowed us to solve an experimental transient 2D inverse problem. Our method has given some satisfactory results in point heat source identification for 4 and even five heat sources. When the location is assumed to be known, the reconstruction of time variations of line heat source strengths is performed using a BEM inverse formulation connecting a future time-steps and a regularization method. Through this experiment, we show the good potentialities of our methodology, connecting BEM and infrared thermography. With our particular experiment we have shown that it is possible to find at least four heat sources with good results and without any internal measurement. The application to 3D heat conduction is more complex due to the difficulty to produce a point source with a sufficient strength to be detected.

References

[1] A.J. Silva Neto, M.N. Ozisik, Two-dimensional inverse heat conduction problem of estimating the time-varying strength of a line heat source, J. Appl. Phys. 71 (1992) 5357–5362.

[2] C.-Yu Yang, The determination of two heat sources in an inverse heat conduction problem, Int. J. Heat Mass Transfer 42 (1999) 345–356.

[3] R. Abou Khachfe, Résolution numérique de problèmes inverses 2D non linéaires de conduction de la chaleur par la méthode des éléments finis et l'algorithme du gradient conjugué- Validation expérimentale, University doctoral thesis, Ecole polytechnique de Nantes, France, 2000.

[4] C. Le Niliot, F. Lefèvre, A method for multiple steady line heat sources identification in a diffusive system: application to an experimental 2D problem, Int. J. Heat Mass Transfer 44 (2001) 1425–1438.

[5] C. Le Niliot, F. Rigollet, D. Petit, An experimental identification of line heat sources in a diffusive system using the boundary element method, Int. J. Heat Mass Transfer 43 (2000) 2205–2220.

[6] C. Le Niliot, F. Lefèvre, Multiple transient point heat sources identification in heat diffusion: application to numerical 2D and 3D problems, Numer. Heat Transfer, Part B 39 (3) (2001) 277–301.

[7] F. Papini, P. Gallet, Thermographie Infrarouge: Image et mesure, Masson, Paris, 1994.

[8] M. Banaszkiewicz, K. Seiferlin, T. Spohn, G. Kargl, N. Kömle, A new method for the determination of thermal conductivity and thermal diffusivity from linear heat source measurements, Rev. Sci. Instrum. 68 (11) (1997) 4184–4190.

[9] W. Elenbaas, The dissipation of heat by free convection from vertical and horizontal cylinders, J. Appl. Phys. 19 (1948) 1148–1154.

[10] C. Le Niliot, The boundary element method for the time varying strength estimation of point heat sources: application to a two-dimensional diffusion system, Numer. Heat Transfer, Part B 33 (1998) 301–321.

[11] C.A. Brebbia, J.C.F. Telles, L.C. Wrobel, Boundary Element Techniques, Springer, New York, 1984.

[12] A.N. Tikhonov, V.Y. Arsenin, Solutions of Ill-posed Problems, V.H. Winston & Sons, Washington, DC, 1977.

[13] J.V. Beck, B. Blackwell, C.R.St. Clair, Inverse Heat Conduction, Ill-posed Problems, Wiley, New York, 1985.

[14] W.H. Press, B.P. Flannery, S.A. Teulossky, W.T. Vetterling, Numerical Recipes, Cambridge University Press, Cambridge, 1999.